Journal of Materials Chemistry C

PAPER

View Article Online
View Journal | View Issue

Cite this: J. Mater. Chem. C, 2014, 2, 4922

Identifying effects of TiO_2 nanowires inside bulk heterojunction organic photovoltaics on charge diffusion and recombination†

P. Yang,[a] D. F. Zeigler,[b] K. C. Bryant,[b] T. R. Martin,[a] D. R. Gamelin[b] and C. K. Luscombe*[a]

Received 20th March 2014
Accepted 29th April 2014

DOI: 10.1039/c4tc00563e

www.rsc.org/MaterialsC

The charge carrier dynamics of poly(3-hexylthiophene) (P3HT):[6,6]-phenyl-C_{61}-butyric acid methyl ester (PCBM) organic bulk-heterojunction photovoltaics with and without TiO_2 nanowires are studied. Using inorganic nanowires as electron transport pathways improves the charge transit time and electron diffusion coefficient, which is the origin of fill factor and power conversion efficiency improvement observed in these devices. Through further comparison of devices with surface-modified nanowires (PCB–TiO_2-NW), it is found that under AM 1.5 light illumination, charge recombination is dominant in the organic layer rather than at the TiO_2 nanowire surface.

Introduction

Conjugated polymer-based organic photovoltaics (OPVs) have attracted great interest as an inexpensive technology for harvesting energy from sunlight.[1–3] The potential low cost of OPVs originates from the solution processability of conjugated polymers. However, there are also drawbacks in using conjugated polymers in photovoltaic applications; the charge transport of OPVs is limited by the low intrinsic charge mobilities, and the power conversion efficiency (PCE) is further limited by the excitons (bound electron–hole pair) that form upon photoexcitation in conjugated polymers. To dissociate the excitons into free charge carriers, they must migrate to an interface between the donor and acceptor materials, and the difference between the lowest unoccupied molecular orbitals (LUMO) of the donor and acceptor must be at least 0.3 eV to overcome the exciton binding energy.[4,5] Excitons can typically only diffuse about 10 nm before decaying.[4,6] As such, well-mixed donor and acceptor phases with dimensions on the order of 20 nm are necessary for efficient exciton dissociation,[7–9] which is why the bulk-heterojunction (BHJ) structure is the most commonly used device architecture.[10–12] However, the tortuous charge transport pathways in BHJs, coupled with the already low intrinsic charge mobilities of the organic materials, yields poor charge transport at the device level thereby limiting device efficiencies.

Recently, we had shown that introducing small quantities of TiO_2 nanowires without surface modifiers into the active layer of BHJ OPVs could improve the PCE in these devices, and by only using a small quantity of TiO_2 nanowires, we were able to maintain the simple one-step solution-processing procedure to prepare the active layer of the devices.[13,14] Moreover, by controlling both the dimension and dispersion of nanowires, we were able to minimize impact of adding nanowires on the active layer morphology.[13,14] Our previous research showed that the PCE improvement was likely a result of the introduction of efficient electron transport pathways in the active layer as indicated by the increased electron mobilities observed by space-charge-limited current (SCLC) measurements.[13,14] Others have shown that the use of TiO_2 nanorods can reduce device performance because of surface traps and defects, and that TiO_2 surface modification is necessarily to suppress recombination.[15,16] To understand the roles of inorganic nanostructures embedded in the active layers of OPVs, a deeper understanding of charge carrier dynamics, such as charge recombination, is required.

One method to probe the charge carrier dynamics of organic–inorganic interfaces is impedance spectroscopy (IS), which involves frequency analysis of a device's AC behavior. IS has been used to look at charge carrier dynamics in dye-sensitized solar cells (DSCs),[17–20] quantum dot solar cells (QDSCs),[21,22] and solid hole conductors.[23,24] More recently, IS has been applied to OPVs by Bisquert *et al.* to obtain recombination lifetimes, charge transit times, and electron diffusion coefficients.[25–27]

In this study, we investigate the charge carrier dynamics in P3HT:PCBM photovoltaic devices with and without TiO_2-NWs using IS. Additionally, the effects of TiO_2-NW surface modification were also examined to assess observations that such

[a]Department of Materials Science and Engineering and Molecular Engineering and Sciences Institute, University of Washington, Box 352120, Seattle, WA 98195-2120, USA. E-mail: luscombe@uw.edu

[b]Department of Chemistry, University of Washington, Box 351700, Seattle, WA 98195-1700, USA

† Electronic supplementary information (ESI) available. See DOI: 10.1039/c4tc00563e

modification is necessary to reduce surface charge trapping[28–30] and back recombination.[15,31,32]

Experimental

Material preparation

TiO_2 nanowires were grown on fluorine-doped tin oxide (FTO) coated glass (TEC 15, Hartford Glass Co.) by hydrothermal synthesis according to a modified literature procedure.[33] Titanium isopropoxide (0.15 g) was added to 10 mL of a 1 : 1 mixture of concentrated hydrochloric acid and water. After stirring for several minutes, the clear colorless solution was decanted into a Teflon lined stainless steel autoclave (45 mL, Parr Instrument Co.). Two FTO slides were placed at an angle inside the vessel with the conductive side facing downwards. The nanowires were grown at 150 °C for 7.5 h to achieve lengths of ~3 μm. Then, the TiO_2-NW was scratched off the substrate, placed in ethanol, and sonicated for at least 3 h. After sonication, the ethanol with TiO_2-NW was drop cast on another glass substrate. Scanning electron microscope (SEM) images were taken to check the separation of TiO_2-NWs. If the TiO_2-NWs were well separated, they were scratched off again and weighed on a balance to get the desired amount.

C_{60}-substitued benzoic acid used in surface modification of nanowires was synthesized according to ref. 34. A mixture of 4-carboxybenzaldehyde, C_{60}, and *N*-methylglycine was dissolved in chlorobenzene, and the solution was refluxed overnight under a nitrogen atmosphere (Scheme 1). The solvent was removed by rotary evaporation under reduced pressure. The product was purified by silica gel column chromatography with toluene to toluene–THF (2 : 1) as the eluents to afford a brown-yellow solid. Then, C_{60}-subsituted benzoic acid was dissolved in THF–ethanol (1 : 1) at 0.2 mg mL^{-1} concentration After the solution was prepared, 0.2 mg mL^{-1} TiO_2-NW was added to start coating, and the mixture was kept stirring and heated at 60 °C for 40 h. Next, this surface-modified TiO_2-NW (PCB–TiO_2-NW) was centrifuged and washed with THF several times to remove any excessive PCB acid. Fourier transform infrared (FTIR) spectra (Fig. S1†) were taken to confirm surface modification.

Device fabrication

ITO-coated glass substrates (15 Ω m^{-2}) were cleaned in an ultrasonic bath with detergent, deionized (DI) water, acetone, and isopropyl alcohol. Substrates were then taken out and dried under N_2 flow followed by air plasma treatment for 15 min. A hole-transport layer of poly(3,4-ethylene-dioxylene thiophene):poly(styrene sulfonic acid) (PEDOT:PSS, Clevios P VP Al 4083) was spin-coated onto the ITO surface from its aqueous solution (40 nm thick). The films were baked at 140 °C for 10 min before being transferred into a nitrogen-filled glovebox. The chlorobenzene solution, which contained 25 mg mL^{-1} P3HT (Reike Metal, Sepiolid P100) and 15 mg mL^{-1} PCBM (American Dye Source Inc. ADS61BFB), was stirred inside the glovebox for at least 3 h at 60 °C. The active layers of control devices were achieved by directly spin-coating the P3HT:PCBM solution to form a 140 nm thick layer. In both NW devices, 0.2 wt% of TiO_2 was added to the P3HT:PCBM solution. For devices with TiO_2-NW, the TiO_2-NW was added into the solution and taken out of the glovebox to sonicate for 30 min. For PCB–TiO_2-NW, the nanowires were dispersed in solution by stirring. This solution was kept stirring before it was spin-coated onto the PEDOT:PSS to achieve the same thickness active layer as the control group. Subsequently, all the devices were transferred into a deposition chamber inside the glovebox and 100 nm of Al were thermally evaporated under a vacuum of 5×10^{-7} Torr. Finally, the devices were completed by annealing at 150 °C for varying times.

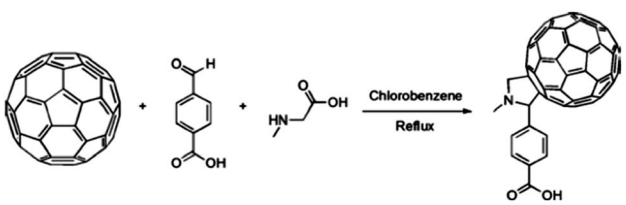

Scheme 1 Synthesis of C_{60}-substitued benzoic acid.

Device characterization

The *J–V* characteristics of the solar cells were tested using a Keithley 2400 source measurement unit, and an Oriel Xenon lamp (450 W) coupled with an AM 1.5 filter (which was used as the light source). The light intensity was determined using a calibrated standard silicon solar cell with a KG5 filter traceable to the National Renewable Energy Laboratory. A light intensity of 100 mW cm^{-2} was used in all of the measurements in this study. Device parameters were obtained by taking the average of at least 20 samples for each processing condition. Impedance spectroscopy (IS) measurements were performed using an Agilent HP 4278A, applying a small voltage perturbation (20 mV rms). Different light intensities were obtained using combinations of absorptive neutral density filters (Thorlabs Inc.). Measurements were carried out at open-circuit voltage condition at each light intensity sweeping frequencies from 1 MHz down to 20 Hz.

Result and discussion

The devices used for both IS and photovoltaic characterization share the same structure: ITO/PEDOT:PSS/active layer/Al. However, IS measurements were taken at varying light intensities while PV measurements were made using a light intensity of 100 mW cm^{-2}. To force the photovoltaic device to operate under recombination conditions, voltages equal to the open-circuit voltage (V_{oc}) at each light intensity were applied so that the photocurrent was nullified by the applied bias.[25] Under this condition, a major RC arc plus additional minor features at higher frequencies characterize the spectra (Fig. 1). At higher frequencies, information regarding transport and series resistance elements can be extracted, while at the lower frequencies, information about recombination in the active layer and thus the effective charge carrier lifetime can be obtained.[25–27]

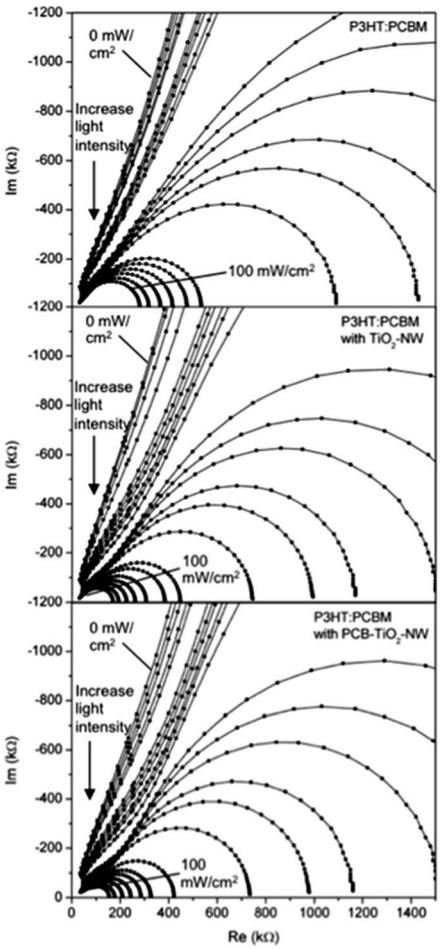

Fig. 1 Impedance spectra of P3HT:PCBM, P3HT:PCBM with TiO_2-NW and P3HT:PCBM with PCB–TiO_2-NW active layers.

In order to obtain quantitative information on carrier dynamics in OPVs, the transmission line model accounting for different impedance responses was employed.[18,25,27] The equivalent circuit in this model (Fig. 2) consists of: (1) distributed resistors representing carrier transport, $r_t = R_t/L$, where L is the active layer thickness; (2) distributed chemical capacitance $c_\mu = C_\mu L$; (3) $r_{rec} = R_{rec}/L$, which accounts for the recombination resistance.[18,27] Furthermore, from these elements, several characteristic parameters related to the charge carrier dynamics in the device can be derived,[18,25,27] such as recombination time (effective carrier lifetime):

$$\tau_{rec} = R_{rec} C_\mu \quad (1)$$

carrier transit time:

$$\tau_{diff} = R_t C_\mu \quad (2)$$

and therefore the charge diffusion coefficient:

$$D_n = \frac{L^2}{\tau_{diff}} \quad (3)$$

The fitting results of R_t, R_{rec} and C_μ for all three devices (Fig. 3) show trends typical of those reported previously for OPVs.[25,35,36] The increase of chemical capacitance with V_{oc} follows the shape of a Gaussian distribution, and in the tested V_{oc} range it reflects the shape of the density of states of electrons.[25,26] Both R_t and R_{rec} of all devices decrease with increasing V_{oc} due to the higher charge carrier density from higher illumination. However, devices with TiO_2-NW and PCB–TiO_2-NW show a faster decay in R_t with increase in charge carrier density, while R_{rec} values are similar in all three devices. Moreover, R_t exceeds R_{rec} above 0.55 V for the three devices, which implies that at higher light intensities (>2.5 mW cm^{-2}), devices are highly recombining for voltages around V_{oc},[37] and that the performance is limited by the transport of carriers.

From the fitting results, the effective carrier lifetime, charge transit time and charge diffusion coefficients were calculated by using eqn (1)–(3), and the results are shown in Fig. 4. The charge carrier density was calculated by integrating the chemical capacitance at a given V_{oc}.[25] Surprisingly, at higher charge densities (>10^{16} cm^{-3}), the effective lifetimes are similar in all three devices, indicating similar recombination rates in all three devices at high illumination intensity (*i.e.* at typical OPV testing conditions) despite the presence of possible surface traps and defects introduced by the TiO_2. However, at lower charge densities (~10^{15} cm^{-3}), the effective lifetime was

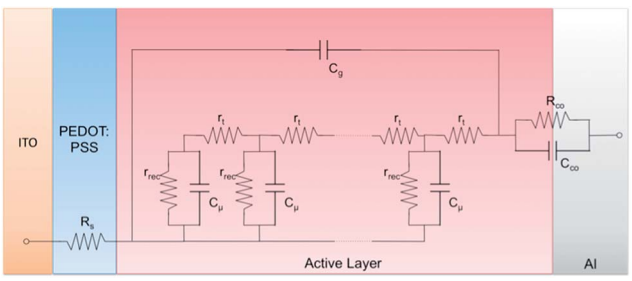

Fig. 2 Transmission line representation of the OPV equivalent circuit used here. Distributed elements related to carrier transport (r_t), recombination (r_{rec}), chemical capacitance (C_μ); series resistance (R_s), R_{co}, C_{co} parallel subcircuit simulates the contact between active layer and top electrode.

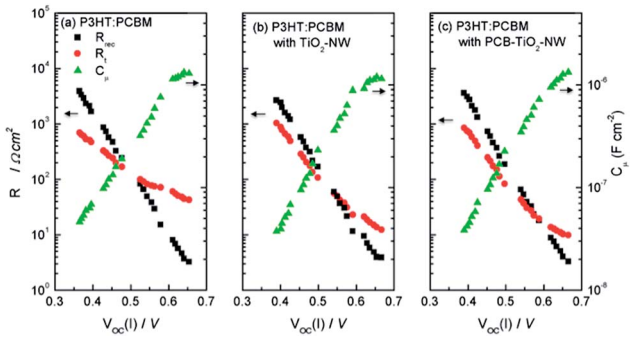

Fig. 3 R_t, R_{rec} and C_μ extracted from fitting the circuit model to the impedance spectra of (a) P3HT:PCBM, (b) P3HT:PCBM with TiO_2-NWs and (c) P3HT:PCBM with PCB–TiO_2-NWs.

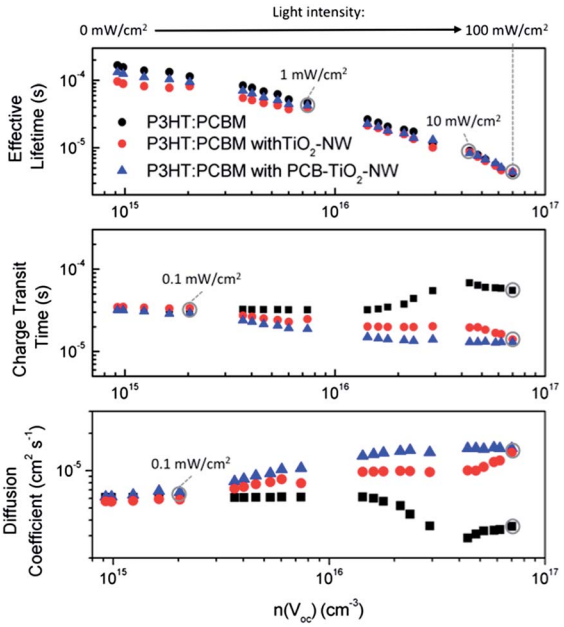

Fig. 4 Effective lifetime (top), charge transit time (middle) and diffusion coefficient (bottom) of devices with P3HT:PCBM, P3HT:PCBM with TiO_2-NWs and P3HT:PCBM with PCB–TiO_2-NWs, plotted as a function of charge carrier density.

observed to be the highest in P3HT:PCBM and lowest in TiO_2-NW containing devices, followed by devices with PCB–TiO_2-NW. The slower recombination rate observed in surface-modified TiO_2-NW compared to the unmodified TiO_2-NW is presumably due to the passivation of surface traps, consistent with previous reports.[31,32,38]

In contrast to the effective carrier lifetimes, nearly one order of magnitude improvements were found in the charge transit time and thus the charge diffusion coefficient of devices with nanowires at higher charge carrier densities, confirming our previous results where enhanced electron mobilities were observed in TiO_2-NW containing devices.[13,14] However, at low charge carrier densities, the charge transit times and the charge diffusion coefficients were the same across all three devices. Additionally, at higher charge densities, an increase in charge diffusion coefficient with increasing charge carrier density was observed for devices with nanowires. The change in the charge transit time and diffusion coefficient in devices with nanowires can be explained by the multiple-trapping model suggested by the previous charge transport studies in nanostructured TiO_2.[39,40] Electrons are mobile only when they de-trap to a high-energy conduction band, or mobility edge. The more electrons injected, the higher the de-trapping rate, and therefore mobility increases.[39,40]

The charge transit times and diffusion coefficients show that at low charge carrier densities, charges move primarily through the organic materials, while at high charge carrier densities, charges move through the TiO_2 nanowires. We speculate that at low charge carrier densities, the charge transfer from the organic to TiO_2 does not occur because of recombination at the NW surface; however, at high charge carrier densities, the TiO_2 surface traps are filled, suppressing recombination and thereby allowing charge transfer to TiO_2. The IS data confirm that recombination is dominant in TiO_2 at low charge carrier densities, while recombination is dominant in the organic at high charge carrier densities (*i.e.* at typical OPV testing conditions).

Fig. 5 shows the *J–V* characteristics of devices with and without nanowires. The important device parameters are summarized in Table 1. Both devices with nanowires show improvement in PCE, and the dominating factor in their efficiency enhancement is the increase in FF. Based on the IS analysis of the aforementioned devices, this increase in FF can be attributed to the improved charge transport afforded by the nanowires. Moreover, slightly higher average J_{sc} values were also found in devices with nanowires. In comparison to devices with TiO_2-NW, devices with PCB–TiO_2-NW exhibit no further improvement in PCE. This result is consistent with their similar effective lifetime, diffusion coefficient and charge transit time at high carrier density obtained from IS measured at 100 mW cm^{-2} light intensity—the same light intensity used in *J–V* characterization. Recombination at the TiO_2 nanowire surface is thus not a dominant factor that affects performance in this set of devices under AM 1.5 light illumination.

Our results contradict those found by others, where surface modification of TiO_2 nanorods yielded substantial increases in PCEs.[15,16] We believe that this difference stems from the fact that only a very small amount of TiO_2 (0.2 wt%) is used in our devices, compared with ~50 wt% in previous studies.[15,16] Moreover, at 3 μm lengths, the NWs have substantially smaller surface-to-volume ratios compared to the ~30 nm × 5 nm nanorods used previously.[15,16] As such, TiO_2 surface traps are rapidly filled with increasing charge carrier density under AM 1.5 illumination, eliminating the need to use surface modifiers. The fact that the diffusion coefficient in PCB–TiO_2-NW containing devices saturates at lower charge carrier densities compared to devices containing TiO_2-NW shows that surface modification does help to a certain extent, just not under typical OPV testing conditions.

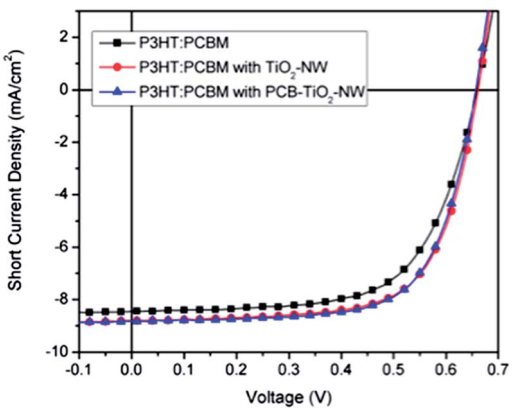

Fig. 5 *J–V* characterization of P3HT:PCBM and P3HT:PCBM OPV devices with embedded TiO_2-NW or PCB–TiO_2-NW electron conduits.

Table 1 Device parameters of P3HT:PCBM and P3HT:PCBM OPV devices with embedded TiO_2-NW or PCB–TiO_2-NW (under AM 1.5, 100 mW cm^{-2})[a]

	V_{oc} (V)	J_{sc} (mA cm^{-2})	FF	PCE (%)
P3HT:PCBM	0.661 (0.009)	8.5 (0.2)	64% (2%)	3.61 (0.04)
P3HT:PCBM with TiO_2-NW	0.662 (0.005)	8.8 (0.1)	68% (1%)	3.95 (0.08)
P3HT:PCBM with PCB–TiO_2-NW	0.658 (0.006)	8.8 (0.1)	69% (1%)	3.98 (0.05)

[a] Numbers in brackets are errors.

Conclusion

By applying IS analysis at open-circuit conditions, the charge carrier dynamics of devices with OPVs containing TiO_2 nanowires were studied. Improvements in the charge transit time and electron diffusion coefficient were directly observed in devices with nanowires, which explains the PCE and FF improvement in the photovoltaic devices. The faster increase in diffusion coefficient as a function of charge carrier density in devices with PCB–TiO_2-NW compared to devices with TiO_2-NW reflects an improved interface between the nanowires and organic materials in the active layer. More importantly, from IS analysis and *J–V* characterization of devices with unfunctionalized and functionalized nanowires, similar diffusion coefficients and charge carrier lifetimes were found at high charge carrier density (*i.e.* under standard 100 mW cm^{-2} light intensity), indicating that by using small quantities of high-aspect-ratio TiO_2 nanowires, recombination at the nanowire surface can be minimized and the nanowires used as efficient charge conduits.

Acknowledgements

This work was supported by the NSF (SOLAR Award DMR 1035196, EFRI-SEED 1038165) and the Research Corporation for Science Advancement.

Notes and references

1 H. Hoppe and N. S. Sariciftci, *J. Mater. Chem.*, 2006, **16**, 45.
2 H. Hoppe and N. S. Sariciftci, *J. Mater. Res.*, 2004, **19**, 1924–1945.
3 C. J. Brabec, S. Gowrisanker, J. J. M. Halls, D. Laird, S. Jia and S. P. Williams, *Adv. Mater.*, 2010, **22**, 3839–3856.
4 N. Greenham, X. Peng and A. Alivisatos, *Phys. Rev. B: Condens. Matter Mater. Phys.*, 1996, **54**, 17628–17637.
5 G. D. Scholes and G. Rumbles, *Nat. Mater.*, 2006, **5**, 683–696.
6 T. Q. Nguyen, V. Doan and B. J. Schwartz, *J. Chem. Phys.*, 1999, **110**, 4068–4078.
7 T. Erb, U. Zhokhavets, G. Gobsch, S. Raleva, B. Stühn, P. Schilinsky, C. Waldauf and C. J. Brabec, *Adv. Funct. Mater.*, 2005, **15**, 1193–1196.
8 F. Demir, N. Brande, B. Mele, S. Bertho, D. Vanderzande, J. Manca and G. Assche, *J. Therm. Anal. Calorim.*, 2011, **105**, 845–849.
9 P. G. Karagiannidis, N. Kalfagiannis, D. Georgiou, A. Laskarakis, N. A. Hastas, C. Pitsalidis and S. Logothetidis, *J. Mater. Chem.*, 2012, **22**, 14624–14632.
10 F. Zhang, K. G. Jespersen, C. Björström, M. Svensson, M. R. Andersson, V. Sundström, K. Magnusson, E. Moons, A. Yartsev and O. Inganäs, *Adv. Funct. Mater.*, 2006, **16**, 667–674.
11 J. K. Lee, W. L. Ma, C. J. Brabec, J. Yuen, J. S. Moon, J. Y. Kim, K. Lee, G. C. Bazan and A. J. Heeger, *J. Am. Chem. Soc.*, 2008, **130**, 3619–3623.
12 H. Xin, X. Guo, G. Ren, M. D. Watson and S. A. Jenekhe, *Adv. Energy Mater.*, 2012, **2**, 575–582.
13 P. Yang, X. Zhou, G. Cao and C. K. Luscombe, *J. Mater. Chem.*, 2010, **20**, 2612–2616.
14 P. Yang, D. K. Zhong, M. Yuan, A. H. Rice, D. R. Gamelin and C. K. Luscombe, *Phys. Chem. Chem. Phys.*, 2013, **15**, 4566–4572.
15 Y.-Y. Lin, T.-H. Chu, S.-S. Li, C.-H. Chuang, C.-H. Chang, W.-F. Su, C.-P. Chang, M.-W. Chu and C.-W. Chen, *J. Am. Chem. Soc.*, 2009, **131**, 3644–3649.
16 H.-C. Liao, C.-H. Lee, Y.-C. Ho, M.-H. Jao, C.-M. Tsai, C.-M. Chuang, J.-J. Shyue, Y.-F. Chen and W.-F. Su, *J. Mater. Chem.*, 2012, **22**, 10589–10596.
17 T. Hoshikawa, R. Kikuchi and K. Eguchi, *J. Electroanal. Chem.*, 2006, **588**, 59–67.
18 J. Bisquert, *J. Phys. Chem. B*, 2002, **106**, 325–333.
19 Q. Wang, S. Ito, M. Grätzel, F. Fabregat-Santiago, I. Mora-Seró, J. Bisquert, T. Bessho and H. Imai, *J. Phys. Chem. B*, 2006, **110**, 25210–25221.
20 J. Bisquert, F. Fabregat-Santiago, I. Mora-Seró, G. Garcia-Belmonte and S. Giménez, *J. Phys. Chem. C*, 2009, **113**, 17278–17290.
21 V. González-Pedro, X. Xu, I. Mora-Seró and J. Bisquert, *ACS Nano*, 2010, **4**, 5783–5790.
22 H. Lee, M. Wang, P. Chen, D. R. Gamelin, S. M. Zakeeruddin, M. Grätzel and M. K. Nazeeruddin, *Nano Lett.*, 2009, **9**, 4221–4227.
23 F. Fabregat-Santiago, J. Bisquert, L. Cevey, P. Chen, M. Wang, S. M. Zakeeruddin and M. Grätzel, *J. Am. Chem. Soc.*, 2009, **131**, 558–562.
24 M. Wang, P. Chen, R. Humphry-Baker, S. M. Zakeeruddin and M. Grätzel, *ChemPhysChem*, 2009, **10**, 290–299.
25 G. Garcia-Belmonte, P. P. Boix, J. Bisquert, M. Sessolo and H. J. Bolink, *Sol. Energy Mater. Sol. Cells*, 2010, **94**, 366–375.
26 F. Fabregat-Santiago, G. Garcia-Belmonte, I. Mora-Seró and J. Bisquert, *Phys. Chem. Chem. Phys.*, 2011, **13**, 9083–9118.

27 T. Ripolles-Sanchis, A. Guerrero, J. Bisquert and G. Garcia-Belmonte, *J. Phys. Chem. C*, 2012, **116**, 16925–16933.
28 M. Jankulovska, T. Berger, S. S. Wong, R. Gómez and T. Lana-Villarreal, *ChemPhysChem*, 2012, **13**, 3008–3017.
29 S. H. Kang, J.-Y. Kim, Y. Kim, H. S. Kim and Y.-E. Sung, *J. Phys. Chem. C*, 2007, **111**, 9614–9623.
30 E. Enache-Pommer, J. E. Boercker and E. S. Aydil, *Appl. Phys. Lett.*, 2007, **91**, 123116.
31 Y.-Y. Lin, T.-H. Chu, C.-W. Chen and W.-F. Su, *Appl. Phys. Lett.*, 2008, **92**, 053312.
32 Y.-C. Huang, J.-H. Hsu, Y.-C. Liao, W.-C. Yen, S.-S. Li, S.-T. Lin, C.-W. Chen and W.-F. Su, *J. Mater. Chem.*, 2011, **21**, 4450–4456.
33 B. Liu and E. S. Aydil, *J. Am. Chem. Soc.*, 2009, **131**, 3985–3990.
34 S. K. Hau, H.-L. Yip, O. Acton, N. S. Baek, H. Ma and A. K.-Y. Jen, *J. Mater. Chem.*, 2008, **18**, 5113–5119.
35 G. Garcia-Belmonte, A. Munar, E. M. Barea, J. Bisquert, I. Ugarte and R. Pacios, *Org. Electron.*, 2008, **9**, 847–851.
36 J. Bisquert, G. Garcia-Belmonte, A. Munar, M. Sessolo, A. Soriano and H. J. Bolink, *Chem. Phys. Lett.*, 2008, **465**, 57–62.
37 J. Bisquert, I. Mora-Sero and F. Fabregat-Santiago, *ChemElectroChem*, 2014, **1**, 289–296.
38 Y. Gao, X. Pu, D. Zhang, G. Ding, X. Shao and J. Ma, *Carbon*, 2012, **50**, 4093–4101.
39 A. Petrozza, C. Groves and H. J. Snaith, *J. Am. Chem. Soc.*, 2008, **130**, 12912–12920.
40 T. Leijtens, J. Lim, J. Teuscher, T. Park and H. J. Snaith, *Adv. Mater.*, 2013, **25**, 3227–3233.